Mitochondria in peroxisome-deficient hepatocytes exhibit impaired respiration, depleted DNA, and PGC-1α independent proliferation

Annelies Peeters[1]*, Abhijit Babaji Shinde[1]*, Ruud Dirkx[1]*, Joél Smet[2], Katrien De Bock[3,4], Marc Espeel[5], Ilse Vanhorebeek[6], Arnaud Vanlander[2], Rudy Van Coster[2], Peter Carmeliet[3,4], Marc Fransen[7], Paul P. Van Veldhoven[7], Myriam Baes[1]

[1]*KU Leuven - University of Leuven, Department of Pharmaceutical and Pharmacological Sciences, Laboratory of Cell Metabolism, B-3000 Leuven, Belgium*
[2]*Department of Paediatrics, Division of Paediatric Neurology and Metabolism, University Hospital Ghent, B-9000 Ghent, Belgium*
[3]*KU Leuven - University of Leuven, Department of Oncology, Laboratory of Angiogenesis and Neurovascular Link, B-3000 Leuven, Belgium*
[4]*VIB, Vesalius Research Center, Laboratory of Angiogenesis and Neurovascular Link, B-3000 Leuven, Belgium;*
[5]*Dept Basic Medical Sciences, UGhent, B-9000 Ghent, Belgium*
[6]*KU Leuven - University of Leuven, Department of Cellular and Molecular Medicine, Laboratory of Intensive Care Medicine, B-3000 Leuven, Belgium*
[7]*KU Leuven - University of Leuven, Department of Cellular and Molecular Medicine, Laboratory for Lipid Biochemistry and Protein Interactions, B-3000 Leuven, Belgium*

**equal contribution*

Corresponding author:
Prof. Dr. Myriam Baes
Laboratory of Cell Metabolism
Department of Pharmaceutical and Pharmacological Sciences
Herestraat 49 O/NII box 823
B-3000 Leuven Belgium
Tel + 32 16 347283
Fax +32 16 347291
e-mail: myriam.baes@pharm.kuleuven.be

ABSTRACT

The tight interrelationship between peroxisomes and mitochondria is illustrated by their cooperation in lipid metabolism, antiviral innate immunity and shared use of proteins executing organellar fission. In addition, we previously reported that disruption of peroxisome biogenesis in hepatocytes severely impacts on mitochondrial integrity, primarily damaging the inner membrane. Here we investigated the molecular impairments of the dysfunctional mitochondria in hepatocyte selective *Pex5* knockout mice. First, by using blue native electrophoresis and in-gel activity stainings we showed that the respiratory complexes were differentially affected with reduction of complexes I and III and incomplete assembly of complex V, whereas complex II and IV were normally active. This resulted in impaired oxygen consumption in cultured *Pex5*$^{-/-}$ hepatocytes. Second, mitochondrial DNA was depleted causing an imbalance in the expression of mitochondrial- and nuclear-encoded subunits of the respiratory chain complexes. Third, mitochondrial membranes showed increased permeability and fluidity despite reduced content of the polyunsaturated fatty acid docosahexaenoic acid. Fourth, the affected mitochondria in peroxisome deficient hepatocytes displayed increased oxidative stress. Acute deletion of PEX5 *in vivo* using adeno-Cre virus phenocopied these effects, indicating that mitochondrial perturbations closely follow the loss of functional peroxisomes in time. Likely to compensate for the functional impairments, the volume of the mitochondrial compartment was increased several fold. This was not driven by PGC-1α but mediated by activation of PPARα, possibly through *c-myc* overexpression. In conclusion, loss of peroxisomal metabolism in hepatocytes perturbs the mitochondrial inner membrane, depletes mitochondrial DNA and causes mitochondrial biogenesis independent of PGC-1α.

KEYWORDS: peroxisomes, mitochondria, mitochondrial DNA, oxidative phosphorylation, biogenesis, PPARα, PGC-1α

INTRODUCTION

Over the years, it has become clear that peroxisomes and mitochondria have a strong interrelation as they exhibit complementary activities, share proteins and communicate with each other. Metabolically, both organelles are involved and cooperate in the degradation of fatty acids [1; 2]. Very long and branched chain fatty acids are shortened in peroxisomes, followed by transfer to the mitochondria for further breakdown. Some of the enzymes participating in β-oxidation such as alpha-methylacyl-CoA racemase are targeted to both organelles [3]. Moreover, both peroxisomes and mitochondria contribute to the detoxification of oxygen radicals generated in cellular processes [4]. In addition, it was recently shown that induction of oxidative stress in peroxisomes affects the mitochondrial redox balance via unresolved mechanisms [5]. These organelles also depend on the same proteins for the execution of their fission process such as Dlp1, Fis1 and Mff1 [6-9]. A defect in Dlp1 can even lead to a combined peroxisomal-mitochondrial disorder [10]. Furthermore, other proteins such as MAVS that are involved in antiviral signalling were shown to reside both on the peroxisomal and outer mitochondrial membrane [11]. A surprising finding was the existence of an intracellular transport route between mitochondria and peroxisomes whereby mitochondria derived vesicles can incorporate selected cargo and fuse with peroxisomes [12-14].

Another illustration of the tight link between these organelles is that mitochondrial abnormalities arise when peroxisomes are dysfunctional. In a few early reports on Zellweger syndrome, the most severe peroxisome biogenesis disorder, mitochondrial abnormalities were documented in hepatocytes. These changes were not studied in detail but included structural alterations at the inner mitochondrial membrane and a reduction in the activities of several complexes of the respiratory chain [15-19]. Importantly, in different Zellweger syndrome mouse models generated by disruption of *Pex5* [20; 21], *Pex2* [22], or *Pex13* [23], swollen mitochondria with sparse and abnormally shaped cristae were found in hepatocytes.

Mitochondrial anomalies were also recapitulated in a liver-selective *Pex5* knockout mouse model (*L-Pex5*$^{-/-}$) that survives into adulthood [24]. These mice develop microvesicular steatosis, hepatomegaly, and fibrosis. The reduced abundance of cristae was accompanied by impaired activity of complex I, III and V as determined by spectrophotometry and by an energetic deficit leading to the activation of the

cellular energy sensor AMPK [25]. In contrast, mitochondrial matrix enzymes were more active in mutant hepatocytes as shown for citrate synthase [24] and mitochondrial β-oxidation [26].

At present, the mechanisms through which peroxisomal inactivity detrimentally impacts on mitochondrial structure and function are unresolved. In order gain insight into these intriguing organellar interactions, we have investigated in more detail the properties of the aberrant mitochondria in peroxisome deficient hepatocytes, including the expression of the respiratory complexes, redox state, lipid composition, fluidity and permeability of the membranes, and DNA content. Furthermore, the time course of mitochondrial impairments was investigated by acutely deleting PEX5 from hepatocytes. Finally, we investigated whether and how compensatory mitochondrial proliferation is activated.

MATERIALS AND METHODS

Mouse breeding

L-Pex5$^{-/-}$ mice were generated by crossing Albumin-Cre and *Pex5*$^{FL/FL}$ mice as previously described [24]. All experiments were performed on 8-15-week-old *Pex5*$^{FL/FL}$, considered as controls and littermate *L-Pex5*$^{-/-}$ mice, unless otherwise stated. *Pex5*$^{FL/FL}$ mice were also brought into a PPARα deficient background (provided by Prof. F. Gonzalez [27]). In some experiments *Pex5* was acutely inactivated in hepatocytes by intravenous administration of adenovirus encoding Cre-recombinase (3.10^9 pfu) or control adenovirus in *Pex5*$^{FL/FL}$ *PPARα*$^{-/-}$ or *Pex5*$^{FL/FL}$ *PPARα*$^{+/+}$ as previously described [25]. Mice were maintained on a 12-hour light/12-hour dark schedule and were fed a standard rodent food chow and water *ad libitum*. All animal experiments were approved by the Institutional Animal Ethical Committee of the University of Leuven.

Analysis of mitochondria

Purification of mitochondria

L-Pex5$^{-/-}$ and wild-type mice were killed by cervical dislocation and livers were rapidly removed, washed in ice-cold homogenization medium (HM) (0.25 M sucrose, 5 mM Mops, 1 mM EDTA, 0.1% (v/v) ethanol, pH 7.2), minced and homogenized in a Potter homogenizer with a motor-driven pestle (1200 rpm). Cellular debris was pelleted by centrifugation of the homogenate at 770g for 10 minutes. The post-nuclear supernatant (PNS) was spun for 10 minutes at 2330g and the pellet was washed once to obtain a fraction enriched in mitochondria. For some experiments, this fraction, corresponding to 1.5 g of liver, was layered on top of a Percoll solution (40% (w/v) Percoll, 0.22 M sucrose, 1 mM Mops, 1 mM EDTA, 0.1 % (v/v) ethanol, pH7.2) and centrifuged for 1 h at 4°C at 34,000g (Beckmann ultracentrifuge) as described before [28] but using only 18 ml of Percoll solution. Subsequently, 500 µl fractions were collected starting from the bottom. The distribution of the organelles was monitored by measurement of marker enzymes [mitochondria (glutamate dehydrogenase, GDH); lysosomes (acid phosphatase); endoplasmic reticulum (glucose-6-phosphatase)]. Mitochondrial enzymes were recovered in fractions 2-22 of the 38 fractions that were collected. The 5 fractions containing the highest activity of the mitochondrial marker enzyme GDH were combined, diluted 20 times in HM, and centrifuged (10 min, 4°C, 2330g). Based on Western blot and EM analysis these fractions primarily contained mitochondria and were only contaminated to a minor extent with peroxisomes, ER or

lysosomes. The purified mitochondrial pellet was resuspended in 1 ml of HM and used immediately or stored at -80°C for further analysis.

Quantification of mitochondria

Purified mitochondria were counted on a FACSCanto flow cytometer (BD) using BD Trucount™ tubes.

Electron microscopy on isolated mitochondria

The Percoll-purified mitochondrial pellet was resuspended in a cell free system (CFS) buffer (10 mM HEPES, 220 mM mannitol, 68 mM sucrose, 2 mM NaCl, 5 mM pyruvate, 0.5 mM EGTA, 2 mM $MgCl_2$, 2.5 mM KH_2PO_4, pH 7.4), centrifuged for 3 min, and fixed in freshly prepared 4% (w/w) glutaraldehyde and 8% (w/v) BSA in CFS buffer for 30 minutes on ice. The pellet was washed with sodium cacodylate buffer supplemented with 1% (w/v) $CaCl_2$ and prepared for electron microscopy.

Blue native gel electrophoresis of the oxidative phosphorylation (OXPHOS) complexes

Blue native gel electrophoresis followed by in-gel activity staining was performed as described [29] on isolated liver mitochondria. Samples of controls and knockouts were loaded in duplicate (60 µg/lane). In the first set of lanes, activity staining of complex I, III and IV was performed, and the second set of lanes was used for the activity staining of complexes II and V. The bands resulting from the complex I, II, III and IV activities were scanned in transmission mode. The complex V band, which was seen as a white precipitate, was scanned in 'reflexion' mode using a dark background for better visualization [29].

Mitochondrial transmembrane potential

The membrane potential of purified mitochondria was analyzed essentially as in [30]. Briefly, purified mitochondrial suspensions were incubated in medium (110 mM KCl, 75 mM mannitol, 20 mM MOPS, 10 mM glutamate, 1 mM malate, 1 mM EGTA, albumin 1 mg/ml, pH 7.2) for 1 min at room temperature in the dark with JC-1 (1.5 µg/mg protein) in a final volume of 0.5 ml. Suspensions were analyzed immediately using a FACSVantage SE flow cytometer (BD) equipped with a single 488 argon laser. The filter in front of the fluorescence 1 (FL1) photo multiplier (PMT) transmits at 530 nm and has a bandwidth of 30 nm, and the filter used in the FL2 channel transmits at 585 and has a bandwidth of 42 nm. To analyze mitochondria stained with JC-1, the PMT value of the detector in both FL1 FL2 PMT was set at 480 V; FL1–FL2 compensation was 1.6 %, and FL2–FL1 compensation was 30%.

Measurement of Fluorescence Anisotropy

Mitochondrial membrane fluidity was evaluated by fluorescence anisotropy of the mitochondria-bound dyes 1,6-diphenyl 1,3,5-hexatriene (DPH) and trimethylammonium (TMA)-DPH according to [31]. Freshly prepared mitochondrial suspensions (0.5 mg/ml) were incubated in Standard Incubation Medium (SIM; 200 mM sucrose, 10 mM Tris-HCl, 1 mM KH_2PO_4, 10 µM EGTA, 3 µM rotenone, 0.5 µg oligomycine and 5 mM succinate; pH 7.4) either with DPH (50 µM; diluted from a stock solution of 20 mM (prepared in tetrahydrofurane) with 10 mM Tris-HCl pH 7.4, 150 mM KCl, 1 mM EDTA) or TMA-DPH (3 µM) for 30 minutes at 37°C, under continuous stirring. Steady-state fluorescence polarization was measured in a Hitachi spectrofluometer (ex 366 nm: em 425 nm). The results are expressed as anisotropy units (r), where $r = (I_0/I_{90})/(I_0+2I_{90})$. I_0 and I_{90} represent the intensities of light when polarizers were in parallel or in perpendicular orientations, respectively. Correction for light scattering and intrinsic fluorescence were routinely made by subtracting the signal obtained from identical but unlabeled samples and the fluorescence of the buffer plus label alone.

Lipid analysis

Lipid extracts were prepared from Percoll purified mitochondria and separated by thin-layer chromatography using heptane/ether/acetic acid (70/30/1, v/v) before enzymatic analysis of triacylglycerols [32], cholesterol and cholesterylesters [33]. Phospholipids were separated by thin-layer chromatography with chloroform/methanol/acetic acid/ formic acid/water (70:30:12:4:2, v/v) as developing solvent [34]. Major spots corresponding to phosphatidylcholine (PC), phosphatidylethanolamine (PE), cardiolipin (CL), phosphatidylserine (PS) and phosphatidylinositol (PI) were visualized with iodine vapour, ninhydrin staining and phosphate staining, scraped and phosphorus content was determined. Ceramides were quantified with recombinant ceramide kinase in presence of ^{32}P-ATP [35; 36].

Total fatty acid composition was determined in lipid extracts or in phospholipids extracted from scraped silica with chloroform/methanol (1:1,v/v) by acidic transmethylation and gas chromatography (SPB-PUFA column; Varian 3800). Individual fatty acids were identified by comparing each peak's retention time to those of external standards, and were expressed as the mol % of total fatty acids.

Estimation of mitochondrial size

EM micrographs of 3 control and *L-Pex5* knockout mouse livers at a magnification of 5200 were used to measure the mitochondrial surface area using the program ImageJ 2.0 (NIH, USA). The values are expressed as Mean ± SEM.

RNA analysis

Quantitative real-time RT-PCR

qRT-PCR was performed as described previously [37] using an ABI PRISM 7500 Real Time PCR instrument (Applied Biosystems, Lennik, Belgium) and probes labelled with the fluorescent dye FAM and quencher TAMRA. Primers and probes were designed using Primer Express Software (Applied Biosystems, Lennik, Belgium) (Supplemental Table 1). Relative expression levels of the target genes were calculated taking into account the amplification efficiency as described [38]. The relative expression levels of the target genes were calculated as a ratio to the housekeeping gene β-actin.

Microarray analysis

The transcriptional profiles of livers of 10-week-old control and *L-Pex5*$^{-/-}$ mice (n=3) were analyzed by using the whole genome Affymetrix GeneChip® Mouse Genome 430 2.0 Array as described previously [39]. Labeling of the samples, hybridization, washing and scanning of the chips was carried out at the MicroArray Facility in Leuven (MAF, Leuven, Belgium). The complete dataset is available under GEO record GSE27720.

Mitochondrial DNA copy number

Nuclear and mitochondrial DNA were isolated from liver tissue using a DNeasy kit (Qiagen). To quantify the mitochondrial DNA (mtDNA)/nuclear DNA (nDNA) ratio, qPCR analysis was performed using primers and probes for the gene encoding mitochondrial 16S ribosomal RNA and nuclear encoded Mpeg, a gene expressed in macrophages (Supplemental Table 1).

Protein analysis

Western blotting

Western blotting was performed as described previously [40]. HRP-labeled secondary antibodies were used and detection was performed using the ECL plus detection kit (Amersham). The following

primary antibodies were used: COX1 (Mitosciences, Abcam), TOM20 (Santa Cruz), VDAC1 (Cell Signaling) and β-actin (Cell Signaling).

Enzyme activity

Glutamate dehydrogenase (GDH), complex I and citrate synthase activities were measured in liver homogenates as described [24]. In order to evaluate the quality/integrity of the Percoll-purified mitochondria, GDH activity was measured in the presence and absence of detergent. For total GDH activities, mitochondria were pre-incubated with 0.017% CHAPS (3-[(3-Cholamidopropyl)dimethylammonio]-1-propanesulfonate) for one minute to destroy mitochondrial membrane barriers.

In vitro analysis

Isolation of primary hepatocytes

Hepatocytes were isolated using a two-step collagenase perfusion technique, plated, and cultured as previously described [26]. For some experiments, primary hepatocytes were infected either 4 hours after plating with adenovirus encoding PGC-1α (MOI=30) [25] or before plating with lentivirus encoding mitochondrial roGFP2 (mt-roGFP2) (MOI=5).

Extracellular flux analysis

Primary hepatocytes, plated at 10,000 cells per well, were analyzed 24h after plating using a Seahorse XF24 flux analyzer (Seahorse Bioscience) as previously described [41]. Oxygen consumption rate (OCR), a measure for electron transport and oxidative phosphorylation, was recorded.

Redox state of mitochondria

Isolated primary hepatocytes from control and *L-Pex5*$^{-/-}$ mice were cultured in 35 mm FluoroDishes (World Precision Instruments, Hertfordshire, England), at a density of 0.5 million cells/dish. To measure superoxide content, hepatocytes were stained after 24 hours with MitoSOX Red (5 µM, 15 minutes), washed with PBS, and subsequently incubated with MitoTracker Green (250 nM, 20 minutes) at 37°C in growth medium. After washing with PBS, medium was refreshed and images were acquired immediately. Absorption/emission maxima for MitoSOX Red and MitoTracker Green were 510/580 nm and 490/516 nm, respectively. As MitoTracker Green stains all the mitochondria irrespective of their redox or membrane potential, the ratio of fluorescent intensities of MitoSOX

Red/MitoTracker Green was used for normalization purposes. In two independent experiments, 10 different cells of each genotype were evaluated in which 10 regions of interest per cell were selected.

To monitor the mitochondrial glutathione redox state a lentiviral vector encoding mt-roGFP2 was generated based on a template provided by Dr. Jim Remington (University of Oregon)[42]. Isolated hepatocytes from control and *L-Pex5*$^{-/-}$ mice were transduced immediately after isolation at a MOI of 5 and cultured in 35/14 mm glass bottom dishes (MatTek corporation, Ashland, USA). After 24 hours, media were refreshed and – 24 hours later - images were acquired at the excitation wavelengths of 400 and 480 nm as described elsewhere [5] . The ratio of fluorescent intensities at 400 to 480 nm can be used as a readout of the glutathione redox environment in the organelle. In three independent experiments, 10-15 different cells of each genotype were evaluated in which 10 regions of interest per cell were selected.

All the images were acquired with a motorized inverted IX-81 microscope connected to a CCD-FV2T digital camera (Olympus, Aartselaar, Belgium) and analyzed as previously described [5].

Statistics

The unpaired two-sided Student's t-test or two-way ANOVA followed by Bonferroni was used to compare the results obtained for both groups of mice.

RESULTS

Defective respiratory chain complexes I, III and V cause impaired mitochondrial respiration in L-Pex5 knockout hepatocytes

We previously determined by spectrophotometric analyses that the ultrastructural anomalies of the mitochondrial inner membrane in livers of *L-Pex5*$^{-/-}$ mice were accompanied by profoundly impaired activities of complex I (to ~ 20% of control), mild reduction of complex III and V (~ 60% of control), whereas complex II and IV were unaltered [24]. This raised the question whether the affected respiratory complexes were present but not functional, or alternatively, whether the assembly/stability of these complexes was compromised. To visualize OXPHOS complexes, blue native gel electrophoresis was performed on isolated liver mitochondria. This revealed a reduction in protein levels of complex I, III and V in the *L-Pex5*$^{-/-}$ livers (Figure 1a) whereas the protein bands of complex II and complex IV were hardly detectable in both wild-type and knockout mitochondria (Figure 1a).

To better visualize the complexes and monitor their functionality, in-gel activity stainings were conducted. In agreement with the spectrophotometric analyses, complex II (Figure 1b right panel) and IV (Figure 1b left panel) showed substantial in-gel activity in the knockout liver although the mobility of these complexes was reduced. Furthermore, the activity of complex III was undetectable in mitochondria from *L-Pex5*$^{-/-}$ livers whereas this was low but clearly present in mitochondria from control mice (Figure 1b left panel). Surprisingly however, although the in-gel activity analyses do not allow precise quantification, complex I activity was only moderately reduced, which is in contrast to the spectrophotometric data. An additional striking finding was that complex V activity was primarily present in several catalytically active subcomplexes (Figure 1b right panel). Such F1 subcomplexes were previously found in patients with mitochondrial disorders [29; 43]. Notably, F1 subcomplexes can be more active than the holo-complex due to the absence of the inhibitor protein IF1 [43]. These data indicate that the residual complex V activity, previously measured by spectrophotometric analysis, was largely attributable to catalytically active subcomplexes that can synthesize ATP but are unable to transport protons.

To investigate the impact of the respiratory complex impairments on O_2 consumption, hepatocytes from control and *L-Pex5*$^{-/-}$ livers were tested in a Seahorse XF24 flux analyzer. Under baseline conditions, the oxygen consumption rate (OCR) was significantly lower in *L-Pex5*$^{-/-}$ than wild-type

hepatocytes (Figure 1c). After addition of antimycin A, an inhibitor of complex III that completely inhibits mitochondrial respiration, oxygen consumption significantly dropped in wild-type hepatocytes, but this inhibitor had little effect on *L-Pex5*$^{-/-}$ hepatocytes, indicating that mitochondrial respiration was already reduced to minimal levels.

Expression of mitochondrially-encoded subunits and mitochondrial DNA content is impaired

To investigate the origin of the differential depletion of the respiratory complexes, the expression of a selected set of subunits encoded by the nuclear and mitochondrial genome was determined by microarray, qRT-PCR and western blot analysis. Based on previously generated microarray data [25; 44], the transcripts of nuclear-encoded subunits were either unaltered or increased (Supplemental Table 2). In contrast, qRT-PCR analysis revealed that transcripts of the mitochondrially-encoded ND1 (complex I), COX2 (complex IV) and ATP6 (complex V) were all significantly suppressed (Figure 2a). This was confirmed at the protein level by reduced expression of COX1 (data not shown). Because a concerted decrease of mitochondrially-encoded mRNAs can be the result of a reduction of mitochondrial DNA, we determined the ratio of mtDNA/nuclear DNA. In *Pex5*$^{-/-}$ livers this ratio was halved compared to littermate controls (Figure 2b). Taken together, loss of mtDNA impaired the expression of mitochondrially-encoded subunits, which contrasts to the normal to increased transcript levels of nuclear-encoded subunits.

The mitochondrial compartment is enlarged in peroxisome deficient liver

Several observations, including the electron microscopy data showing clusters of mitochondria [24] and the increased activity of mitochondrial matrix enzymes [24; 26], suggested that the volume of the mitochondrial compartment was increased in hepatocytes of *L-Pex5* knockout mice. In order to better document this phenomenon, mitochondria were purified by differential and Percoll gradient centrifugation. As shown in Figure 3a, the peak of the mitochondrial GDH activity shifted to lower density fractions in the knockout preparations, likely reflecting their aberrant morphology. Both from control and knockout preparations, we used the five fractions containing the highest GDH activity for further experiments.

The enlargement of the mitochondrial compartment in peroxisome deficient hepatocytes was proven by several lines of evidence. First, the pellet containing the mitochondria isolated from *Pex5* knockout

livers was considerably larger (0.17 ± 0.03 g/g liver vs 0.10 ± 0.01 g/g liver in wild-type; n=6, $p<0.05$) and contained more protein (19 ± 2 mg/g liver vs 12 ± 1.5 mg/g liver for wild-type, n=6, $p<0.05$) and phospholipids (3.6 ± 0.3 µmol/g liver vs 1.4 ± 0.3 µmol/g liver, n=6, $p<0.001$). Interestingly, the ratio of phospholipids/protein was significantly increased (189.9 ± 3.4 nmol/mg proteins for knockout vs 115.6 ± 4.2 nmol/mg proteins for wild-type; n=6, $p<0.001$), probably pointing to an altered content of the mitochondrial compartment. This increase in mass of isolated mitochondria was not caused by a larger size of individual mitochondria in the knockout liver as estimated by measuring the surface area of mitochondria on electron micrographs (Figure 3b). Second, counting of purified mitochondria using FACS analysis yielded a 3-fold higher number of mitochondria than controls (Figure 3c). Third, in line with these findings, microarray analysis revealed increased expression of genes encoding mitochondrial matrix (Citrate synthase, Malate dehydrogenase 2, Isocitrate dehydrogenase 2) and membrane proteins (including TOM20, TIM10, prohibitin, CPT2), as shown in supplemental Table 2. This was further confirmed by a 2-4 fold increase in the activity per g liver for mitochondrial matrix enzymes, GDH and citrate synthase, and the increased protein levels of outer mitochondrial membrane proteins TOM20 and VDAC1 using western blot analysis (Figure 3d). Thus, the increased number of mitochondria is in sharp contrast with the reduced level of mtDNA/nuclear DNA, implying that the amount of DNA per mitochondrion is severely depleted.

Mitochondria isolated from L-Pex5 knockout mice retain their structural and functional abnormalities

To further characterize the features of isolated mitochondria from peroxisome deficient livers, we performed additional structural and functional tests. Electron microscopic analysis of Percoll purified mitochondrial fractions revealed that mitochondria from wild-type mice were present in either an orthodox or condensed configuration (Figure 4a), reflecting respectively metabolic state III and IV [45-47]. In contrast, mitochondria from *L-Pex5* knockout livers were not found in either conformation. In some mitochondria, the matrix was reduced to a concentric ring, and large empty spaces, presumably intermembrane space, could be observed (Figure 4a).

Subsequently, we tested whether Percoll purified mitochondria still showed a reduction of the mitochondrial membrane potential, as previously observed in primary hepatocytes from *L-Pex5* knockout mice [24]. After incubating freshly purified mitochondria with JC1, almost all control

mitochondria displayed a high membrane potential (Figure 4b). In clear contrast, almost all knockout mitochondria emitted a green fluorescent signal, pointing to a low membrane potential. In addition, complex I activity measured by spectrophotometric analysis was undetectable in knockout mitochondria (wild-type values: 0.125 U/mg protein). Thus, pure mitochondrial fractions retained the functional anomalies seen *in vivo* and in cell culture.

Purified mitochondria of L-Pex5 knockout mice display increased membrane fluidity

The shift in the sedimentation of the knockout mitochondria in Percoll gradients reflects a change in buoyant density, caused either by changes in the composition and/or by altered permeability of the inner membrane. In order to evaluate the integrity of the isolated mitochondria, GDH activity was measured in the presence and absence of detergents. A large amount appeared to be non-latent (Figure 4c) pointing to changes in the dynamics of the mitochondrial membrane.

To obtain a more direct readout of the mitochondrial membrane fluidity, we analyzed the changes in the steady state fluorescence polarization of mitochondria bound to DPH (a fluorescent dye that is readily incorporated in the hydrophobic region of the phospholipid bilayer) or TMA-DPH (a fluorescent probe, which becomes incorporated in the membrane surface between the phospholipid headgroups). The rotational diffusion freedom of these probes was monitored by measuring the extent of depolarization of the exciting polarized light [48]. Percoll-purified knockout mitochondria showed lower fluorescence polarisation of DPH as compared to control mitochondria (Figure 4d). Similar results were obtained using TMA-DPH (data not shown). These results indicate that the mitochondrial membrane fluidity and thus mitochondrial membrane dynamics were abnormally increased in *Pex5* knockout mitochondria.

The lipid composition of mitochondrial membranes is altered in peroxisome deficient hepatocytes

Since membrane fluidity is strongly influenced by changes in cholesterol content and fatty acid composition of the membrane [49-51], lipidomic analysis of the Percoll-purified mitochondria was performed. The stoichiometry of the major membrane components was determined. Despite normal cholesterol content in total liver, the ratio of cholesterol per phospholipid was decreased in knockout compared to control mitochondria (10.0 ± 0.5 vs 12.6 ± 0.6 nmol/ 100 nmol phospholipid; n=4,

p<0.05), in line with the increased membrane fluidity. Ceramide levels did however not statistically differ between control and knockout mitochondria (82 ± 9 vs 68 ± 13 pmol/nmol phospholipid, respectively). Subsequently, we quantified the relative amounts of the different phospholipid classes. The proportion of phosphatidylcholine (PC), phosphatidylethanolamine (PE), cardiolipin (CL), phosphatidylserine (PS) or phosphatidylinositol (PI) was not significantly altered (Figure 4e). Lysophospholipids, known to affect the membrane permeability, were not detected by thin layer chromatography.

Finally, the fatty acid composition of Percoll-purified mitochondria and of the phospholipids PC, PE and CL was determined using GC analysis (Supplemental Table 3). In general, the balance between saturated, monounsaturated, and polyunsaturated fatty acids did not differ much between control and knockout mitochondria. However, some major changes in individual fatty acids were found in all samples examined. Docosahexaenoic acid levels (DHA, $C_{22:6n-3}$) were reduced by 80% in purified knockout mitochondria and in all major phospholipid classes. This can be ascribed to the inactivity of peroxisomal β-oxidation, necessary for the final step in the synthesis of this compound. This was accompanied by a compensatory increase of $C_{18:2}$ levels. The replacement of a PUFA with a di-unsaturated fatty acid in fact reduces the double bond index and is in conflict with increased fluidity of the mitochondrial membrane.

Increased oxidative stress in mitochondria of peroxisome deficient hepatocytes

Malfunctioning of the respiratory chain can be accompanied by altered production of ROS and oxidative stress. Previously, we did not find evidence for oxidative stress development in *Pex5*$^{-/-}$ hepatocytes based on measurements of peroxide levels with dichlorodihydrofluorescein diacetate in isolated hepatocytes [24]. To specifically evaluate the redox state of mitochondria, we now used more targeted and specific probes. First, to detect superoxide levels, the most common ROS species generated in mitochondria [52], cultured hepatocytes were incubated with MitoSOX Red. This analysis revealed that the fluorescence signal was significantly lower in knockout than control mitochondria (Figure 5a). However, this is likely due to impaired uptake of the probe in mitochondria as a result of the reduced membrane potential. Subsequently, mt-roGFP2, a mitochondrially targeted glutathione redox sensor [42], was transduced in mitochondria of control and *Pex5*$^{-/-}$ hepatocytes by lentiviral infection. This analysis showed a significant increase of the mitochondrial redox state in knockout

hepatocytes (Figure 5b), indicating that the mitochondrial anomalies were accompanied by increased oxidative stress.

Acute elimination of peroxisomes causes similar mitochondrial alterations

All the above experiments were performed using livers of adult mice in which peroxisomal function was chronically deleted from hepatocytes since birth [24]. To exclude the possibility that these results reflected a long-term adaptation to the peroxisome deficiency state, we also acutely eliminated PEX5 in hepatocytes. This also allowed us to delineate the timing of mitochondrial anomalies subsequent to loss of peroxisomal function. To this end adenoviral Cre recombinase was administered to *Pex5*$^{FL/FL}$ mice, using previously described methods [25]. Upon deletion of PEX5, no new functional peroxisomes can be formed and the existing peroxisomes disappear with an estimated 2-day half-life [53]. By monitoring urate oxidase, the activity of which strongly depends on its peroxisomal localization, we observed that 7 days after induction of PEX5 deletion, functional peroxisomes had partially disappeared. One week later, the majority of hepatocytes was devoid of intact peroxisomes (Figure 6a). This was confirmed by the cytosolic staining pattern of the peroxisomal marker enzyme catalase (data not shown).

Analysis of key mitochondrial features revealed that acute depletion of peroxisomes in hepatocytes induced similar mitochondrial defects as chronic loss, further highlighting that these defects were primary in nature. This analysis revealed that the activity of complex I, measured by spectrophotometry, and expression levels of COX2 and ND1 were still normal one week after adenoviral Cre administration. However, after two weeks, complex I activity was strongly impaired (2.5 ± 0.2 mU/mg protein after injection of adenoviral Cre-recombinase versus 8.0 ± 0.3 mU/mg protein with control virus) (Figure 6b, left columns). In addition, expression of COX2 and ND1 (Figure 6c) and the mtDNA abundance (Figure 6d) were significantly decreased at this time point. This was accompanied by ultrastructural abnormalities of mitochondria similar to those in *L-Pex5* knockout livers (data not shown). The mitochondrial anomalies were thus not a long-term adaptation to the absence of functional peroxisomes as they occurred rapidly after peroxisome deletion.

Mitochondrial proliferation in hepatocytes with acute and chronic PEX5 elimination is not driven by PGC1α but is mediated by PPARα

Given that PGC-1α is a major driver of mitochondrial biogenesis and oxidative capacity in conditions of energy deficit by inducing and co-activating crucial transcription factors, it was surprising that transcript and protein levels of PGC-1α were reduced ([25] and Figure 7a) in mice with either a chronic or acute elimination of PEX5 (30- 50% of WT). To obtain insight in the mechanisms causing the enlargement of the mitochondrial compartment, we analyzed the expression of other factors, known to be involved in the regulation of mitochondrial proliferation, respiration or transcription [54] by using qRT-PCR analysis (Figure 7a) and analysing micro-array data of *L-Pex5*$^{-/-}$ livers (Supplemental Table 2).

The expression of the other PGC family members, PGC-1β and PRC1 was unaltered. Also the transcription factors NRF-1 and NRF-2 that coordinate the expression of nuclear-encoded mitochondrial proteins and the mitochondrial transcriptional machinery, and factors that regulate mitochondrial transcription (mitochondrial RNA polymerase and the mitochondrial transcription factor A (TFAM), B1 and B2) were not changed to a significant extent. Notably, transcripts of C-MYC, known to regulate mitochondrial biogenesis [55], were 7-fold increased in *Pex5*$^{-/-}$ livers (Figure 7a). Although the expression of ERRα was unchanged based on micro-array analysis, a significant 1.6 fold increase was noticed by qPCR.

In order to further substantiate these data, mitochondrial biogenesis was also examined in mouse livers with acute elimination of PEX5 using adenoviral Cre recombinase. Notably, mitochondrial expansion was already observed two weeks after induction of *Pex5* recombination as evident from increased activity of citrate synthase (Figure 7b). The expression levels of NRF2 (1.7 fold) and C-MYC (3 fold) were significantly increased in these livers (Figure 7c-d), whereas NRF1 and ERRα were unaltered (data not shown) and TFAM was even reduced (Figure 7e) (to 70% of control).

Interestingly, *c-myc* is known to be induced by PPARα agonists [56] and this nuclear receptor is strongly activated in *L-Pex5*$^{-/-}$ livers [25]. In order to investigate whether PPARα activation was involved in the development of the mitochondrial alterations, a mouse strain was generated with peroxisome deficient hepatocytes in a PPARα null background. Therefore, adenoviral Cre-recombinase was administered to *PPARα*$^{-/-}$*Pex5*$^{FL/FL}$ mice and, as controls, to *PPARα*$^{+/+}$*Pex5*$^{FL/FL}$ mice. In the PPARα deficient background, mitochondria were not proliferating at 2 weeks after administering Cre recombinase, when functional peroxisomes are eliminated, based on normal citrate synthase activity (Figure 7b). Under these circumstances, *c-myc* transcripts were not increased in PEX5 deleted

hepatocytes (Figure 7d), suggesting that both the increase in *c-myc* and mitochondrial proliferation depended on PPARα. In order to examine whether the mitochondrial functional deficits may also be related to PPARα induction, complex I activity was monitored by spectrophotometry. However, 2 weeks after administering Cre recombinase, loss of PEX5 was accompanied by reduced complex I activity that was similar in a *PPARα*$^{-/-}$ (to 29 ± 7% of control) and a *PPARα*$^{+/+}$ background (to 31 ± 3 % of control). Taken together, the strong PPARα activation in peroxisome deficient hepatocytes does not underlie the mitochondrial dysfunction but is involved in the proliferative response.

.

DISCUSSION

The communication between cellular compartments (like mitochondria and peroxisomes) and their interdependence is currently still only poorly understood. We previously documented that peroxisome dysfunction in murine *Pex5*$^{-/-}$ hepatocytes severely impacts on the mitochondrial inner membrane with loss and structural changes of cristae and selective impairment of some but not all activities of OXPHOS complexes [21; 24]. The key novel findings of our study are: 1) mitochondrial membranes displayed altered physicochemical properties; 2) respiratory complexes were differentially depleted or incompletely assembled; 3) mtDNA was reduced leading to an imbalance between mitochondrial- and nuclear-encoded subunits; and 4) the compensatory increase of the mitochondrial compartment was not driven by classical PGC-1α signalling but mediated by PPARα.

Whereas metabolism in the mitochondrial matrix was preserved and even increased in *Pex5*$^{-/-}$ hepatocytes [26], the architecture, function and lipid composition of the inner membrane was severely disorganised. By using blue native gel electrophoresis and in-gel activity analysis, we showed that the abundance of protein in the respiratory complex I and III was respectively moderately and strongly reduced and that the majority of complex V was incompletely assembled. It is remarkable that the activity of complex I (NADH:ubiquinone reductase) was decreased to a larger extent using spectrophotometric analysis (<30% of controls) than using in-gel activity measurements. However, it should be noted that these techniques rely on different enzymatic evaluations of complex I. The spectrophotometric assay measures the complete electron transfer in complex I, i.e. from the substrate NADH to co-enzyme Q. In contrast, the in-gel activity staining of complex I only evaluates the first part of this electron transfer cascade as a hydrogen and electron from NADH are transferred to nitro blue tetrazolium by the action of the flavoprotein subunits located at the peripheral arm of complex I. Furthermore, it has been demonstrated that the CoQ binding site is situated at the interface between the membrane section containing the mtDNA encoded subunits and the peripheral arm of complex I. Importantly, also in patients with mutations in mtDNA-encoded subunits of complex I, the same discrepancy between these two assays has been reported [57; 58]. Therefore, spectrophotometry is better suited to detect defects in the mtDNA encoded subunits of complex I.

The question arises what the precise sequence of events is at the inner mitochondrial membrane. It is indeed unclear whether the loss or assembly defects of the respiratory complex elicited the

malformation of cristae or whether membrane anomalies prevented the integration of respiratory complexes. With regard to the first possibility, studies in yeast documented that defective complex assembly can impair cristae formation. For example, ATP synthase occurs as long rows of dimers at cristae ridges and the inability to dimerize results in the formation of mitochondria with onion-like cristae [59; 60]. In addition, complete loss of mtDNA in the rho^0 mutants causes structural mitochondrial distortions [61] that remarkably resemble those seen in the isolated mitochondria from *Pex5* mutant mice. In PEX5 deficient hepatocytes, the mtDNA copy number per mitochondrion was estimated to be reduced to approximately 15-20%, taking into account the 50% reduced levels of mtDNA/nuclear DNA and the substantial increase in mitochondrial mass (~3 fold). The ensuing decreased levels of mitochondrially-encoded OXPHOS subunits is expected to impair the respiratory complex assembly, which may in turn compromise cristae formation. In particular, for complex V, the two mitochondrially-encoded subunits, a and A6L, are part of the F0 domain embedded in the inner membrane and are necessary for the connection with the catalytically active F1 domain [29]. It was shown that tissues from patients with mtDNA alterations, including mutations in the mitochondrially-encoded *ATP6* or *ATP8* genes, mutations in mitochondrially-encoded tRNA's, specific mtDNA deletions and finally with mtDNA depletion, contain catalytically active subcomplexes of complex V visible by in-gel ATPase activity analysis [29; 43]. This is similar to our findings in peroxisome-deficient hepatocytes where complex V almost exclusively occurs as incomplete subcomplexes concurring with the loss of mtDNA. The intact activity of complex II that contains no mitochondrially encoded subunits further supports the possibility that mtDNA defects are the source of the anomalies. Conversely, complex IV activity was also unaffected when tested by spectrophotometric and in-gel activity analysis albeit the mobility seemed to be reduced. Yet, complex IV depends on 3 mtDNA subunits (COX1-3) questioning how it can assemble and function properly.

However, the most pertinent question in this scenario is how inactive peroxisomes can affect mtDNA. A possible mechanism is through the production of oxidative stress as it is well known that ROS can impair mitochondrial DNA integrity and dysfunctional peroxisomes might be a source of ROS species [4]. Interesting in this respect, excessive oxidative stress generated in peroxisomes increases the mitochondrial but not the cytosolic redox state [5]. It was also reported that lack of ABCD1, a peroxisomal transporter of β-oxidation substrates, causes oxidative damage to mitochondrial proteins leading to reduced activity of ATP synthase but not of other OXPHOS complexes in spinal cord [62]. It

is, however, unclear whether in conditions of peroxisome biogenesis defects, in which both the ROS generating oxidases and the ROS degrading enzymes such as catalase are absent from peroxisomes, ROS species are increased in the cell. Previously, we did not find evidence for increased cellular oxidative stress in *Pex5* deficient hepatocytes [24] whereas we now demonstrated an increase in the redox state of mitochondria. Unfortunately, we could not pinpoint whether this derives from local superoxide production. Indeed, the fluorescence signal using the MitoSOX Red assay was markedly reduced but this may be an underestimation due to the low mitochondrial membrane potential that impairs uptake of the probe [63]. In addition, the depletion of mtDNA in *Pex5* deficient hepatocytes may further weaken the fluorescent signal of the oxidized probe, as this is strongly enhanced by binding to DNA [63]. Therefore, it remains an open question whether the increased redox state of mitochondria is a cause or a consequence of OXPHOS disturbances.

In the alternative hypothesis, peroxisome dysfunction initially causes a morphological insult at the inner membrane preventing the integration of OXPHOS complexes that subsequently are inactive and/or disintegrate. The putative triggering factor could be an imbalance of lipids as a result of impaired peroxisomal metabolism. This could for example explain the presence of the catalytically active F1 domain of complex V that resides in the matrix while the transmembrane subunits a and A6L cannot be incorporated in the membrane due to lipid alterations preventing the formation of the holocomplex. The conserved activity of the small complex II, consisting of only 4 subunits and not integrally embedded in the inner membrane, could be a notable exception as it may remain stable when not properly inserted in the membrane. Again, the normal activity of the large complex IV in spectrophotometric analyses is difficult to reconcile with this mechanism as the majority of its subunits are transmembrane proteins of the inner membrane. According to this rationale, the loss of mtDNA must also be secondary to the inner membrane perturbation. The mitochondrial genome that is packaged in nucleoids [64] is tethered to the inner membrane [65; 66], and it is plausible that the extensive distortion of the inner membrane precludes attachment of the mitochondrial genome, leading to its loss. Interestingly, in some rare cases of inborn errors of metabolism, mutations in enzymes involved in lipid metabolism were shown to cause mitochondrial deficits including loss of mtDNA. Examples are MEGDHEL syndrome due to mutations in SERAC1, involved in phospholipid remodelling and intracellular cholesterol transport [67], Megaconial Congenital Muscular Dystrophy

(MDCMC) caused by choline kinase B deficiency [68] and Sengers syndrome due to a lack of acylglycerolkinase [69; 70].

The altered mitochondrial membrane features in peroxisome deficient liver are further characterized by increased permeability and fluidity. The marked reduction of the poly-unsaturated fatty acid DHA, a product of peroxisomal β-oxidation, in all phospholipid species including cardiolipin is in fact in disagreement with increased membrane fluidity. However, the decreased cholesterol/phospholipid ratio and the loss of respiratory complexes may also contribute to the altered membrane characteristics. Another apparently controversial observation is that, despite an extensive loss of the potential over the inner membrane previously observed in cultured hepatocytes [24] and now in isolated mitochondria, matrix enzymes can still be imported. For example, the mt-roGFP2 probe used to study the intramitochondrial redox balance was efficiently imported into the organelle. In addition, the activities of the mitochondrial matrix proteins GDH and CS were even increased, reflecting the larger mitochondrial mass. Note that these observations are in accordance with previous findings in mtDNA-deficient rho^0 mutants, in which the import and activity of nuclear-encoded proteins is unaffected [61].

Besides enhanced activity of matrix enzymes, the expansion of the mitochondrial compartment in peroxisome deficient hepatocytes was also illustrated by increased organelle numbers and by increased protein content in the mitochondrial fraction. This mitochondrial expansion seemed to be a compensatory response as was also observed in other conditions of mtDNA depletion [71] or defects in mitochondrial respiratory function [72]. Proliferation appeared to be a prompt reaction after acute PEX5 elimination as it occurred concomitant with loss of functional peroxisomes and disruption of the inner membrane. In view of the strong proliferative response, it is most surprising and puzzling that levels of PGC-1α, the master regulator of mitochondrial biogenesis in conditions of energy deficits, are markedly reduced [25]. The family members PGC-1β and PGC-1-related coactivator (PRC) were normally expressed or only slightly induced, not likely to steer proliferation. Therefore, other factors must drive the increased generation of mitochondria. c-MYC is a good candidate as it was reported to induce mitochondrial biogenesis [73; 74] and in addition is a PPARα target gene that was strongly induced in PEX5 deficient liver. This assumption is supported by the absence of *c-myc* induction and mitochondrial proliferation after acute elimination of PEX5 in a PPARα deficient background. In other

conditions of mitochondrial damage [75; 76], increased expression of the transcription factors NRF-1/NRF-2, that play an integrative role in the bigenomic expression of mitochondrial proteins, and their target *Tfam,* that is essential for mtDNA transcription initiation*,* was shown to enhance OXPHOS. Remarkably, no consistent upregulation of these factors was observed at the RNA level in hepatocytes with either acute or chronic deletion of PEX5. Thus, the mechanisms governing the increase of mitochondrial volume in peroxisome deficient hepatocytes as a compensation for respiratory dysfunction deviate from those in other conditions of cellular energy deficits. In particular, the coordinate induction of the mitochondrial and nuclear-encoded proteins seems to fail. At present, it cannot be excluded that the enlarged mitochondrial volume is in part also due to impaired mitophagy, a possibility that needs investigation.

In conclusion, we showed that inactive peroxisomes in hepatocytes impact the mitochondrial genome, the physicochemical properties of the inner membrane, OXPHOS complexes, and the mitochondrial redox state. The triggering factors arising from inactive hepatic peroxisomes and the precise sequence of events in the affected mitochondria need to be further clarified. This is of importance as hepatic pathology, including hepatomegaly and fibrosis, is a cardinal feature in Zellweger syndrome, the prototype peroxisome biogenesis disorder. This hepatopathy may originate from the mitochondrial and not peroxisomal metabolic deficits.

ACKNOWLEDGMENTS

The excellent technical help of Benno Das, Lies Pauwels, Els Meyhi, Gerd Van der Hoeven, Stanny Asselberghs, and Sabine Wyns is gratefully acknowledged. We are indebted to the late Vic Van Duppen for expert help with FACS analysis. We thank Prof. Y. Engelborghs for the use of the spectrofluorometer. This work was funded by grants from Fonds Wetenschappelijk Onderzoek Vlaanderen (G.0760.09 and G.0666.06), Geconcerteerde Onderzoeksacties (2004/08), OT (08/40), and the European Union (LSHG-CT-2004-512018, FP6).

FIGURE LEGENDS

Figure 1: Differential reduction of OXPHOS complexes causes impaired respiration in *Pex5*$^{-/-}$ hepatocytes.

a: Blue native gel electrophoresis shows reduced protein levels of complex I, III and V in *Pex5*$^{-/-}$ liver mitochondria (red arrows). Lane M contains a human skeletal muscle control sample. Complex II and IV are difficult to identify in the liver samples and run with slightly lower mobility as compared to the muscle sample. Representative experiment out of 2 with similar results **b:** In-gel activity staining of respiratory complexes. Left: the function of complex I is moderately reduced whereas complex III is not detectable in *Pex5*$^{-/-}$ liver mitochondria. The blue band above complex III in the control samples represents complex V from the Coomassie staining after blue native electrophoresis. Complex IV is active but displays impaired mobility. Right: the majority of complex V activity is present in lower MW subcomplexes (red arrows) while complex II displays normal function but slightly impaired and variable mobility. Representative experiment out of 4 with similar results **c:** Oxygen consumption was measured in primary hepatocytes. The profiles shown are from 1 experiment in which 10 replicate wells were monitored from either wild type or *Pex5*$^{-/-}$ hepatocytes. *Pex5*$^{-/-}$ hepatocytes consume less oxygen and oxygen consumption is insensitive to the complex III inhibitor antimycin A. Values are shown as mean ± SEM. $p<0.001$: ***; $p<0.01$: ** *L-Pex5*$^{-/-}$ versus control mice.

Figure 2: Reduced expression of mitochondrial-encoded subunits of OXPHOS complexes and of mtDNA in L-*Pex5*$^{-/-}$ mice.

a: Transcript levels of the mitochondrial-encoded subunits ND1 (complex I), COX2 (complex IV) and ATP6 (complex V) were significantly lower in *Pex5*$^{-/-}$ livers as compared to controls (Ct). **b:** Mitochondrial DNA copy number, relative to genomic DNA, was reduced in *Pex5*$^{-/-}$ livers. Values are shown as mean ± SEM for $n \geq 4$. $p<0.001$: ***; $p<0.01$: **; $p<0.05$: * *L-Pex5*$^{-/-}$ versus control mice.

Figure 3: The mitochondrial compartment is enlarged in *L-Pex5*$^{-/-}$ mice.

a: Percoll gradient of mitochondrial-enriched fraction obtained by differential centrifugation of livers from control (Ct) and *L-Pex5*$^{-/-}$ *liver.* The GDH-activity in the first 22 Percoll fractions is shown in U/mg protein. The total GDH-activity was increased in isolated mitochondria of *L-Pex5*$^{-/-}$ mice and the peak of GDH activity shifted towards lower density fractions (1 representative experiment out of 4 is shown). **b:** Mitochondrial area was estimated on electron micrographs at a magnification of 5200 fold by using

the ImageJ program. All values are represented as mean ± SEM of arbitrary units (n= 260 and 160 mitochondria from 3 independent mice from control and *L-Pex5* knockout mice respectively, p<0.05); **c:** Mitochondrial number, determined by FACS analysis, was strongly increased in *L-Pex5*$^{-/-}$ mice. Values shown are mean ± SEM (n = 4, *: p<0.05) **d:** Western blot analysis of the outer mitochondrial membrane proteins TOM20 and VDAC1 shows increased expression relative to β-actin in *L-Pex5*$^{-/-}$ liver as compared to control. Numbers at the top of the blots indicate the fold change as quantified after normalization with β-actin. All values are shown as mean ± SEM (n = 3). p<0.01: **; p<0.05: * *L-Pex5*$^{-/-}$ versus control mice.

Figure 4: Characteristics of Percoll-purified mitochondria of *L-Pex5*$^{-/-}$ mice.

a: EM analysis of GDH-enriched Percoll fractions. Wild-type mitochondria are either in the condensed or orthodox state (marked with X in Ct), while none of the mitochondria from mutant hepatocytes can be found in either state. Unusual conformations of mitochondria from mutant liver are marked with X. **b:** FACS-scan analysis of the mitochondrial membrane potential. The majority of the wild-type mitochondria display a red fluorescence, while KO mitochondria mainly display a green fluorescent signal. The data in this figure are from one experiment out of 4 with similar results. **c:** Non-latent activity measurement of GDH. Values are expressed as % of total GDH-activity ± SEM (n=5). **d:** Anisotropy measurements using DPH as fluorescent probe shows increased fluidity of mitochondrial membranes from *L-Pex5*$^{-/-}$ mice (n=3). **e:** The phospholipid composition of mitochondria is not significantly different in *L-Pex5*$^{-/-}$ compared to control mice. Values are expressed relative to the total amount of phospholipids ± SEM (n=4). PC: phosphatidylcholine, PI: phosphatidylinositol, PS: phosphatidylserine, PE: phosphatidylethanolamine, CL: cardiolipin. p<0.001: ***; p<0.05: * *L-Pex5*$^{-/-}$ versus control mice.

Figure 5: Increased redox state of mitochondria in peroxisome-deficient hepatocytes

a: Ratio of fluorescent intensities of MitoSOX Red (MSR) to mitotracker green (MTG) in primary hepatocytes isolated from control (Ct) and *L-Pex5*$^{-/-}$ mice (n≥200 regions of interest for each genotype derived from 2 independent experiments). **b:** Increased mitochondrial glutathione redox balance in *L-Pex5*$^{-/-}$ primary hepatocytes compared to control hepatocytes as observed by the ratio of fluorescence intensities at 400 and 480 excitation wavelengths of mt-roGFP2 (n≥450 regions of interest for each

genotype derived from 3 independent experiments). Values are expressed as mean ± SEM. p<0.001: *** *L-Pex5*$^{-/-}$ versus control mice.

Figure 6: Acute deletion of PEX5 affects the respiratory chain and mtDNA

a: The declining activity of urate oxidase in liver homogenates of *Pex5*$^{FL/FL}$ mice 7 and 14 days after administration of adenoviral Cre versus control virus is indicative of impaired peroxisomal function. **b-d:** Analyses of mitochondrial markers in liver of *Pex5*$^{FL/FL}$ mice 14 days after administration of adenoviral Cre or control virus. The activity of complex I (**b**), transcript levels of the mitochondrial-encoded subunits COX2 and ND1 (**c**) and the ratio of mtDNA/nuclear DNA (**d**) was significantly decreased in mice treated with adenoviral Cre. Values are expressed as mean ± SEM. p<0.001: ***; p<0.05: * control virus versus adenoviral Cre.

Figure 7: Mitochondrial proliferation in *L-Pex5*$^{-/-}$ livers occurs despite reduced levels of PGC-1α but depends on PPARα

a: qRT-PCR analysis of key regulators of mitochondrial biogenesis and transcription in *L-Pex5*$^{-/-}$ mice with chronic deletion of PEX5. **b:** Citrate synthase activity is increased 14 days after acute deletion of PEX5 with adenoviral Cre recombinase in *Pex5*$^{FL/FL}$ mice but not in a *PPARα*$^{-/-}$ background indicating that mitochondrial proliferation depends on PPARα. **c-e:** qRT-PCR analysis of regulators of mitochondrial biogenesis and transcription in *PPARα*$^{+/+}$*Pex5*$^{FL/FL}$ or *PPARα*$^{-/-}$*Pex5*$^{FL/FL}$ mice 14 days after administering adenoviral Cre recombinase. All values are shown as mean ± SEM (n=4) p<0.001: ***; p<0.01: **; p<0.05: * knockout versus respective control mice.

REFERENCES

1. Wanders RJ (2013) Peroxisomes in human health and disease: metabolic pathways, metabolite transport, interplay with other organelles and signal transduction. Subcell Biochem 69: 23-44
2. Van Veldhoven PP (2010) Biochemistry and genetics of inherited disorders of peroxisomal fatty acid metabolism. J Lipid Res 51: 2863-2895
3. Amery L, Fransen M, De Nys K, Mannaerts GP, Van Veldhoven PP (2000) Mitochondrial and peroxisomal targeting of 2-methylacyl-CoA racemase in humans. J Lipid Res 41: 1752-1759
4. Fransen M, Nordgren M, Wang B, Apanasets O (2012) Role of peroxisomes in ROS/RNS-metabolism: implications for human disease. Biochim Biophys Acta 1822: 1363-1373
5. Ivashchenko O, Van Veldhoven PP, Brees C, Ho YS, Terlecky SR, Fransen M (2011) Intraperoxisomal redox balance in mammalian cells: oxidative stress and interorganellar cross-talk. Mol Biol Cell 22: 1440-1451
6. Kobayashi S, Tanaka A, Fujiki Y (2007) Fis1, DLP1, and Pex11p coordinately regulate peroxisome morphogenesis. Exp Cell Res 313: 1675-1686
7. Camoes F, Bonekamp NA, Delille HK, Schrader M (2009) Organelle dynamics and dysfunction: A closer link between peroxisomes and mitochondria. J Inherit Metab Dis 32: 163-180

8. Delille HK, Alves R, Schrader M (2009) Biogenesis of peroxisomes and mitochondria: linked by division. Histochem Cell Biol 131: 441-446

9. Schrader M (2006) Shared components of mitochondrial and peroxisomal division. Biochim Biophys Acta 1763: 531-541

10. Waterham HR, Koster J, van Roermund CW, Mooyer PA, Wanders RJ, Leonard JV (2007) A lethal defect of mitochondrial and peroxisomal fission. N Engl J Med 356: 1736-1741

11. Dixit E, Boulant S, Zhang Y, Lee AS, Odendall C, Shum B, Hacohen N, Chen ZJ, Whelan SP, Fransen M, Nibert ML, Superti-Furga G, Kagan JC (2010) Peroxisomes are signaling platforms for antiviral innate immunity. Cell 141: 668-681

12. Neuspiel M, Schauss AC, Braschi E, Zunino R, Rippstein P, Rachubinski RA, Andrade-Navarro MA, McBride HM (2008) Cargo-selected transport from the mitochondria to peroxisomes is mediated by vesicular carriers. Curr Biol 18: 102-108

13. Andrade-Navarro MA, Sanchez-Pulido L, McBride HM (2009) Mitochondrial vesicles: an ancient process providing new links to peroxisomes. Curr Opin Cell Biol 21: 560-567

14. Braschi E, Goyon V, Zunino R, Mohanty A, Xu L, McBride HM (2010) Vps35 mediates vesicle transport between the mitochondria and peroxisomes. Curr Biol 20: 1310-1315

15. Goldfischer S, Moore CL, Johnson AB, Spiro AJ, Valsamis MP, Wisniewski HK, Ritch RH, Norton WT, Rapin I, Gartner LM (1973) Peroxisomal and mitochondrial defects in the cerebro-hepato-renal syndrome. Science 182: 62-64

16. Trijbels JM, Berden JA, Monnens LA, Willems JL, Janssen AJ, Schutgens RB, van den Broek-Van Essen M (1983) Biochemical studies in the liver and muscle of patients with Zellweger syndrome. Pediatr Res 17: 514-517

17. Mathis RK, Watkins JB, Szczepanik-Van Leeuwen P, Lott IT (1980) Liver in the cerebro-hepato-renal syndrome: defective bile acid synthesis and abnormal mitochondria. Gastroenterology 79: 1311-1317

18. Hughes JL, Poulos A, Robertson E, Chow CW, Sheffield LJ, Christodoulou J, Carter RF (1990) Pathology of hepatic peroxisomes and mitochondria in patients with peroxisomal disorders. Virchows Arch A Pathol Anat Histopathol 416: 255-264

19. Pfeifer U, Sandhage K (1979) [Light and electron microscopic liver changes in the cerebro-hepato-renal syndrome of Zellweger (Peroxisome deficiency) (author's transl)]. Virchows Arch A Pathol Anat Histol 384: 269-284

20. Baes M, Gressens P, Baumgart E, Carmeliet P, Casteels M, Fransen M, Evrard P, Fahimi D, Declercq PE, Collen D, van Veldhoven PP, Mannaerts GP (1997) A mouse model for Zellweger syndrome. Nat Genet 17: 49-57

21. Baumgart E, Vanhorebeek I, Grabenbauer M, Borgers M, Declercq PE, Fahimi HD, Baes M (2001) Mitochondrial alterations caused by defective peroxisomal biogenesis in a mouse model for Zellweger syndrome (PEX5 knockout mouse). Am J Pathol 159: 1477-1494

22. Keane MH, Overmars H, Wikander TM, Ferdinandusse S, Duran M, Wanders RJ, Faust PL (2007) Bile acid treatment alters hepatic disease and bile acid transport in peroxisome-deficient PEX2 Zellweger mice. Hepatology 45: 982-997

23. Maxwell M, Bjorkman J, Nguyen T, Sharp P, Finnie J, Paterson C, Tonks I, Paton BC, Kay GF, Crane DI (2003) Pex13 inactivation in the mouse disrupts peroxisome biogenesis and leads to a Zellweger syndrome phenotype. Mol Cell Biol 23: 5947-5957

24. Dirkx R, Vanhorebeek I, Martens K, Schad A, Grabenbauer M, Fahimi D, Declercq P, Van Veldhoven PP, Baes M (2005) Absence of peroxisomes in mouse hepatocytes causes mitochondrial and ER abnormalities. Hepatology 41: 868-878

25. Peeters A, Fraisl P, van den Berg S, Ver Loren van Themaat E, Van Kampen A, Rider MH, Takemori H, van Dijk KW, Van Veldhoven PP, Carmeliet P, Baes M (2011) Carbohydrate metabolism is perturbed in peroxisome-deficient hepatocytes due to mitochondrial dysfunction, AMP-activated protein kinase (AMPK) activation, and peroxisome proliferator-activated receptor gamma coactivator 1alpha (PGC-1alpha) suppression. J Biol Chem 286: 42162-42179

26. Dirkx R, Meyhi E, Asselberghs S, Reddy J, Baes M, Van Veldhoven PP (2007) Beta-oxidation in hepatocyte cultures from mice with peroxisomal gene knockouts. Biochem Biophys Res Commun 357: 718-723

27. Lee SS, Pineau T, Drago J, Lee EJ, Owens JW, Kroetz DL, Fernandez-Salguero PM, Westphal H, Gonzalez FJ (1995) Targeted disruption of the alpha isoform of the

peroxisome proliferator-activated receptor gene in mice results in abolishment of the pleiotropic effects of peroxisome proliferators. Mol Cell Biol 15: 3012-3022

28. Van Veldhoven P, Mannaerts GP (1985) Comparison of the activities of some peroxisomal and extraperoxisomal lipid-metabolizing enzymes in liver and extrahepatic tissues of the rat. Biochem J 227: 737-741

29. Smet J, Seneca S, De Paepe B, Meulemans A, Verhelst H, Leroy J, De Meirleir L, Lissens W, Van Coster R (2009) Subcomplexes of mitochondrial complex V reveal mutations in mitochondrial DNA. Electrophoresis 30: 3565-3572

30. Cazzalini O, Lazze MC, Iamele L, Stivala LA, Bianchi L, Vaghi P, Cornaglia A, Calligaro A, Curti D, Alessandrini A, Prosperi E, Vannini V (2001) Early effects of AZT on mitochondrial functions in the absence of mitochondrial DNA depletion in rat myotubes. Biochem Pharmacol 62: 893-902

31. Colell A, Garcia-Ruiz C, Morales A, Ballesta A, Ookhtens M, Rodes J, Kaplowitz N, Fernandez-Checa JC (1997) Transport of reduced glutathione in hepatic mitochondria and mitoplasts from ethanol-treated rats: effect of membrane physical properties and S-adenosyl-L-methionine. Hepatology 26: 699-708

32. Van Veldhoven PP, Swinnen JV, Esquenet M, Verhoeven G (1997) Lipase-based quantitation of triacylglycerols in cellular lipid extracts: requirement for presence of detergent and prior separation by thin-layer chromatography. Lipids 32: 1297-1300

33. Van Veldhoven PP, Meyhi E, Mannaerts GP (1998) Enzymatic quantitation of cholesterol esters in lipid extracts. Anal Biochem 258: 152-155

34. Steenbergen R, Nanowski TS, Nelson R, Young SG, Vance JE (2006) Phospholipid homeostasis in phosphatidylserine synthase-2-deficient mice. Biochim Biophys Acta 1761: 313-323

35. Van Overloop H, Gijsbers S, Van Veldhoven PP (2006) Further characterization of mammalian ceramide kinase: substrate delivery and (stereo)specificity, tissue distribution, and subcellular localization studies. J Lipid Res 47: 268-283

36. Van Overloop H, Denizot Y, Baes M, Van Veldhoven PP (2007) On the presence of C2-ceramide in mammalian tissues: possible relationship to etherphospholipids and phosphorylation by ceramide kinase. Biol Chem 388: 315-324

37. Bottelbergs A, Verheijden S, Hulshagen L, Gutmann DH, Goebbels S, Nave KA, Kassmann C, Baes M (2010) Axonal integrity in the absence of functional peroxisomes from projection neurons and astrocytes. GLIA 58: 1532-1543

38. Giulietti A, Overbergh L, Valckx D, Decallonne B, Bouillon R, Mathieu C (2001) An overview of real-time quantitative PCR: applications to quantify cytokine gene expression. Methods 25: 386-401

39. Martens K, Ver Loren van Themaat E, van Batenburg MF, Heinaniemi M, Huyghe S, Van Hummelen P, Carlberg C, Van Veldhoven PP, Van Kampen A, Baes M (2008) Coordinate induction of PPAR alpha and SREBP2 in multifunctional protein 2 deficient mice. Biochim Biophys Acta 1781: 694-702

40. Baes M, Huyghe S, Carmeliet P, Declercq PE, Collen D, Mannaerts GP, Van Veldhoven PP (2000) Inactivation of the peroxisomal multifunctional protein-2 in mice impedes the degradation of not only 2-methyl-branched fatty acids and bile acid intermediates but also of very long chain fatty acids. J Biol Chem 275: 16329-16336

41. Wu M, Neilson A, Swift AL, Moran R, Tamagnine J, Parslow D, Armistead S, Lemire K, Orrell J, Teich J, Chomicz S, Ferrick DA (2007) Multiparameter metabolic analysis reveals a close link between attenuated mitochondrial bioenergetic function and enhanced glycolysis dependency in human tumor cells. Am J Physiol Cell Physiol 292: C125-136

42. Hanson GT, Aggeler R, Oglesbee D, Cannon M, Capaldi RA, Tsien RY, Remington SJ (2004) Investigating mitochondrial redox potential with redox-sensitive green fluorescent protein indicators. J Biol Chem 279: 13044-13053

43. Carrozzo R, Wittig I, Santorelli FM, Bertini E, Hofmann S, Brandt U, Schagger H (2006) Subcomplexes of human ATP synthase mark mitochondrial biosynthesis disorders. Ann Neurol 59: 265-275

44. Peeters A, Swinnen JV, Van Veldhoven PP, Baes M (2011) Hepatosteatosis in peroxisome deficient liver despite increased beta-oxidation capacity and impaired lipogenesis. Biochimie 93: 1828-1838

45. Scalettar BA, Abney JR, Hackenbrock CR (1991) Dynamics, structure, and function are coupled in the mitochondrial matrix. Proc Natl Acad Sci U S A 88: 8057-8061

46. Hackenbrock CR (1968) Ultrastructural bases for metabolically linked mechanical activity in mitochondria. II. Electron transport-linked ultrastructural transformations in mitochondria. J Cell Biol 37: 345-369

47. Hackenbrock CR (1966) Ultrastructural bases for metabolically linked mechanical activity in mitochondria. I. Reversible ultrastructural changes with change in metabolic steady state in isolated liver mitochondria. J Cell Biol 30: 269-297

48. Van Blitterswijk WJ, Van Hoeven RP, Van der Meer BW (1981) Lipid structural order parameters (reciprocal of fluidity) in biomembranes derived from steady-state fluorescence polarization measurements. Biochim Biophys Acta 644: 323-332

49. Spector AA, Yorek MA (1985) Membrane lipid composition and cellular function. J Lipid Res 26: 1015-1035

50. Mari M, Caballero F, Colell A, Morales A, Caballeria J, Fernandez A, Enrich C, Fernandez-Checa JC, Garcia-Ruiz C (2006) Mitochondrial free cholesterol loading sensitizes to TNF- and Fas-mediated steatohepatitis. Cell Metab 4: 185-198

51. Thewke D, Kramer M, Sinensky MS (2000) Transcriptional homeostatic control of membrane lipid composition. Biochem Biophys Res Commun 273: 1-4

52. Sena LA, Chandel NS (2012) Physiological roles of mitochondrial reactive oxygen species. Mol Cell 48: 158-167

53. Huybrechts SJ, Van Veldhoven PP, Brees C, Mannaerts GP, Los GV, Fransen M (2009) Peroxisome dynamics in cultured mammalian cells. Traffic 10: 1722-1733

54. Scarpulla RC (2008) Transcriptional paradigms in mammalian mitochondrial biogenesis and function. Physiol Rev 88: 611-638

55. Peck B, Ferber EC, Schulze A (2013) Antagonism between FOXO and MYC Regulates Cellular Powerhouse. Front Oncol 3: 96

56. Shah YM, Morimura K, Yang Q, Tanabe T, Takagi M, Gonzalez FJ (2007) Peroxisome proliferator-activated receptor alpha regulates a microRNA-mediated signaling cascade responsible for hepatocellular proliferation. Mol Cell Biol 27: 4238-4247

57. Dermaut B, Seneca S, Dom L, Smets K, Ceulemans L, Smet J, De Paepe B, Tousseyn S, Weckhuysen S, Gewillig M, Pals P, Parizel P, De Bleecker JL, Boon P, De Meirleir L, De Jonghe P, Van Coster R, Van Paesschen W, Santens P (2010) Progressive myoclonic

epilepsy as an adult-onset manifestation of Leigh syndrome due to m.14487T>C. J Neurol Neurosurg Psychiatry 81: 90-93

58. Wray CD, Friederich MW, du Sart D, Pantaleo S, Smet J, Kucera C, Fenton L, Scharer G, Van Coster R, Van Hove JL (2013) A new mutation in MT-ND1 m.3928G>C p.V208L causes Leigh disease with infantile spasms. Mitochondrion 13: 656-661

59. Strauss M, Hofhaus G, Schroder RR, Kuhlbrandt W (2008) Dimer ribbons of ATP synthase shape the inner mitochondrial membrane. The EMBO Journal 27: 1154-1160

60. Sauvanet C, Duvezin-Caubet S, di Rago JP, Rojo M (2010) Energetic requirements and bioenergetic modulation of mitochondrial morphology and dynamics. Semin Cell Dev Biol 21: 558-565

61. Holmuhamedov E, Jahangir A, Bienengraeber M, Lewis LD, Terzic A (2003) Deletion of mtDNA disrupts mitochondrial function and structure, but not biogenesis. Mitochondrion 3: 13-19

62. Lopez-Erauskin J, Galino J, Ruiz M, Cuezva JM, Fabregat I, Cacabelos D, Boada J, Martinez J, Ferrer I, Pamplona R, Villarroya F, Portero-Otin M, Fourcade S, Pujol A (2013) Impaired mitochondrial oxidative phosphorylation in the peroxisomal disease X-linked adrenoleukodystrophy. Hum Mol Genet 22: 3296-3305

63. Robinson KM, Janes MS, Beckman JS (2008) The selective detection of mitochondrial superoxide by live cell imaging. Nat Protoc 3: 941-947

64. Prachar J (2010) Mouse and human mitochondrial nucleoid--detailed structure in relation to function. Gen Physiol Biophys 29: 160-174

65. Albring M, Griffith J, Attardi G (1977) Association of a protein structure of probable membrane derivation with HeLa cell mitochondrial DNA near its origin of replication. Proc Natl Acad Sci U S A 74: 1348-1352

66. Nass MM (1969) Mitochondrial DNA. I. Intramitochondrial distribution and structural relations of single- and double-length circular DNA. J Mol Biol 42: 521-528

67. Sarig O, Goldsher D, Nousbeck J, Fuchs-Telem D, Cohen-Katsenelson K, Iancu TC, Manov I, Saada A, Sprecher E, Mandel H (2013) Infantile mitochondrial hepatopathy is a cardinal feature of MEGDEL syndrome (3-methylglutaconic aciduria type IV with

sensorineural deafness, encephalopathy and Leigh-like syndrome) caused by novel mutations in SERAC1. Am J Med Genet A 161: 2204-2215

68. Castro-Gago M, Dacruz-Alvarez D, Pintos-Martinez E, Beiras-Iglesias A, Delmiro A, Arenas J, Martin MA, Martinez-Azorin F (2014) Exome sequencing identifies a CHKB mutation in Spanish patient with Megaconial Congenital Muscular Dystrophy and mtDNA depletion. Eur J Paediatr Neurol

69. Mayr JA, Haack TB, Graf E, Zimmermann FA, Wieland T, Haberberger B, Superti-Furga A, Kirschner J, Steinmann B, Baumgartner MR, Moroni I, Lamantea E, Zeviani M, Rodenburg RJ, Smeitink J, Strom TM, Meitinger T, Sperl W, Prokisch H (2012) Lack of the mitochondrial protein acylglycerol kinase causes Sengers syndrome. Am J Hum Genet 90: 314-320

70. Calvo SE, Compton AG, Hershman SG, Lim SC, Lieber DS, Tucker EJ, Laskowski A, Garone C, Liu S, Jaffe DB, Christodoulou J, Fletcher JM, Bruno DL, Goldblatt J, Dimauro S, Thorburn DR, Mootha VK (2012) Molecular diagnosis of infantile mitochondrial disease with targeted next-generation sequencing. Sci Transl Med 4: 118ra110

71. Wredenberg A, Wibom R, Wilhelmsson H, Graff C, Wiener HH, Burden SJ, Oldfors A, Westerblad H, Larsson NG (2002) Increased mitochondrial mass in mitochondrial myopathy mice. Proc Natl Acad Sci U S A 99: 15066-15071

72. Than TA, Lou H, Ji C, Win S, Kaplowitz N (2011) Role of cAMP-responsive element-binding protein (CREB)-regulated transcription coactivator 3 (CRTC3) in the initiation of mitochondrial biogenesis and stress response in liver cells. J Biol Chem 286: 22047-22054

73. Li F, Wang Y, Zeller KI, Potter JJ, Wonsey DR, O'Donnell KA, Kim JW, Yustein JT, Lee LA, Dang CV (2005) Myc stimulates nuclearly encoded mitochondrial genes and mitochondrial biogenesis. Mol Cell Biol 25: 6225-6234

74. Scarpulla RC (2011) Metabolic control of mitochondrial biogenesis through the PGC-1 family regulatory network. Biochim Biophys Acta 1813: 1269-1278

75. Suliman HB, Carraway MS, Welty-Wolf KE, Whorton AR, Piantadosi CA (2003) Lipopolysaccharide stimulates mitochondrial biogenesis via activation of nuclear respiratory factor-1. J Biol Chem 278: 41510-41518

76. Miranda S, Foncea R, Guerrero J, Leighton F (1999) Oxidative stress and upregulation of mitochondrial biogenesis genes in mitochondrial DNA-depleted HeLa cells. Biochem Biophys Res Commun 258: 44-49

Figure 1

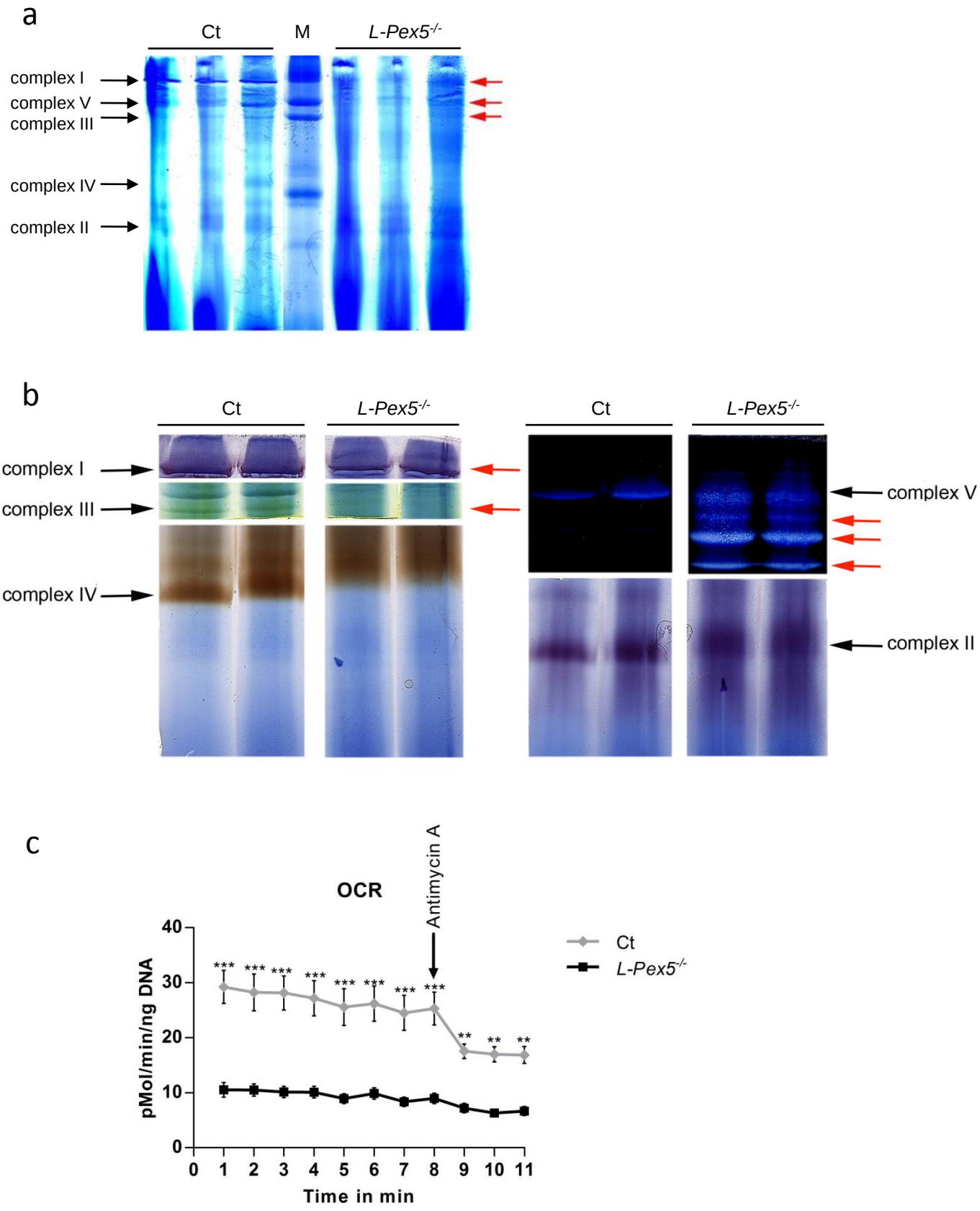
a
Ct
M
L-Pex5-/-
complex I
complex V
complex III
complex IV
complex II
b
Ct
L-Pex5-/-
Ct
L-Pex5-/-
complex I
complex III
complex IV
complex V
complex II
c
OCR
Antimycin A
pMol/min/ng DNA
Time in min
Ct
L-Pex5-/-

Figure 2

a

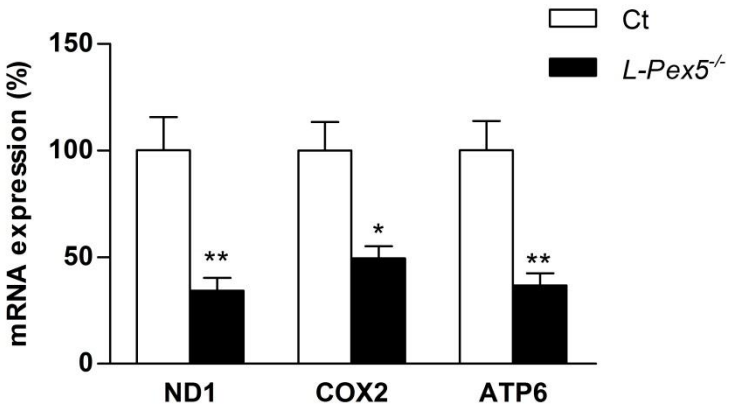
Ct
L-Pex5-/-
mRNA expression (%)
150
100
50
0
**
*
**
ND1
COX2
ATP6

b

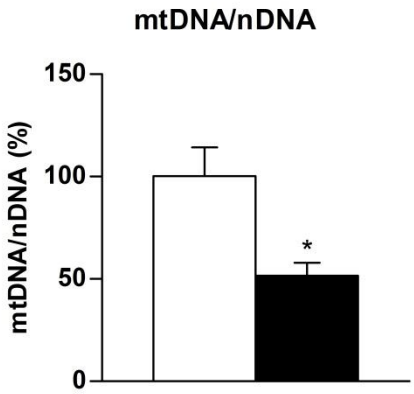
mtDNA/nDNA
mtDNA/nDNA (%)
150
100
50
0
*

Figure 3

a

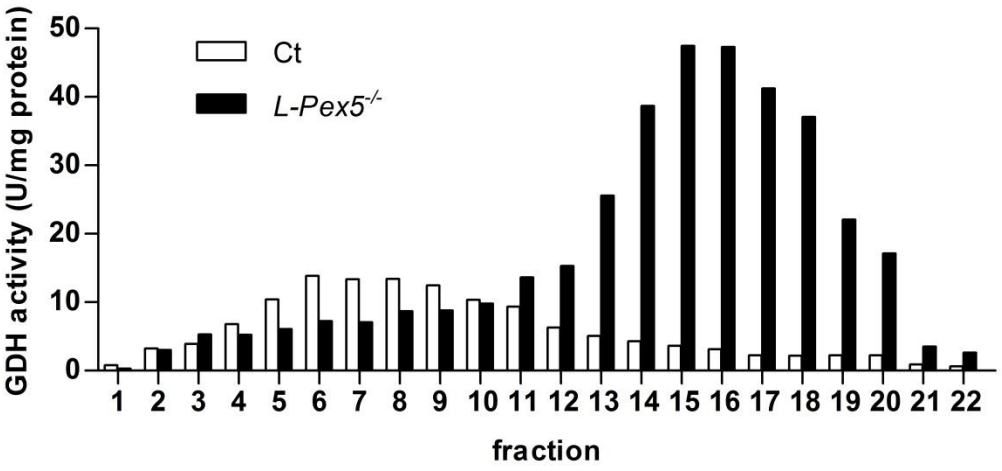

b

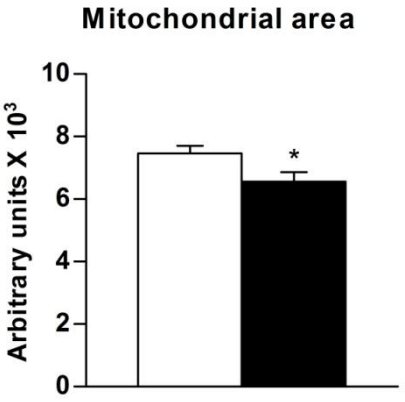

c

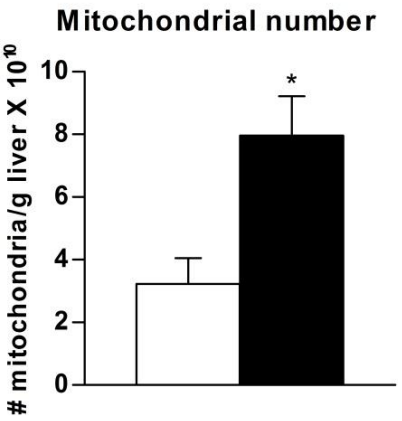

d

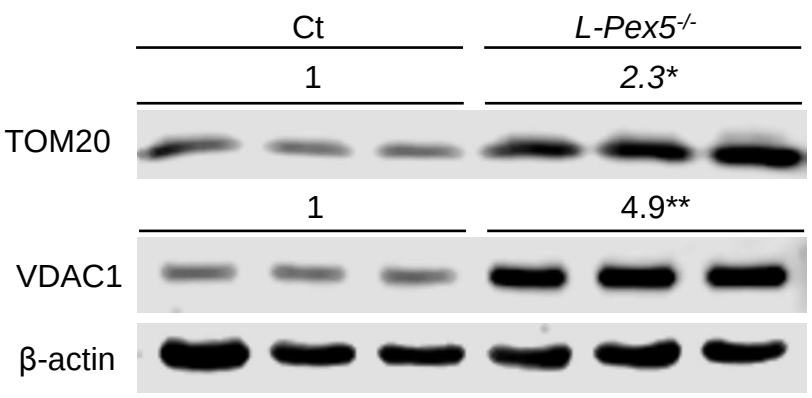

Figure 4

a

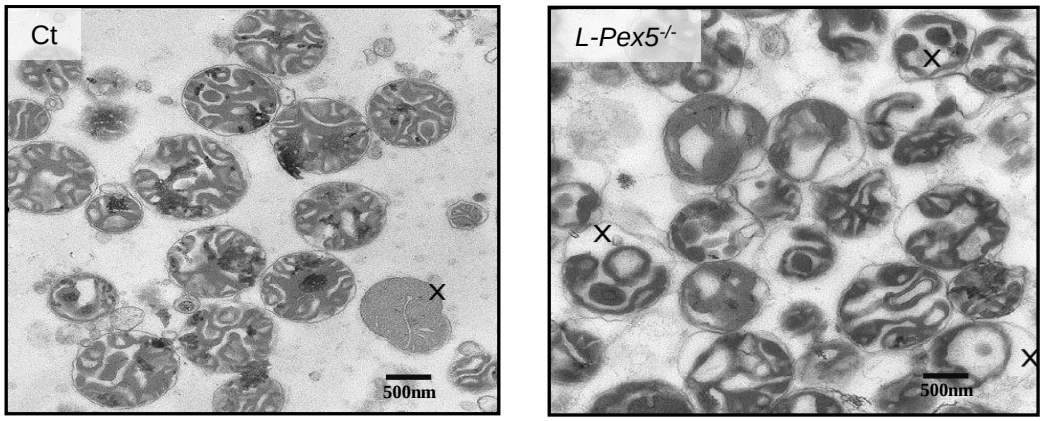

b

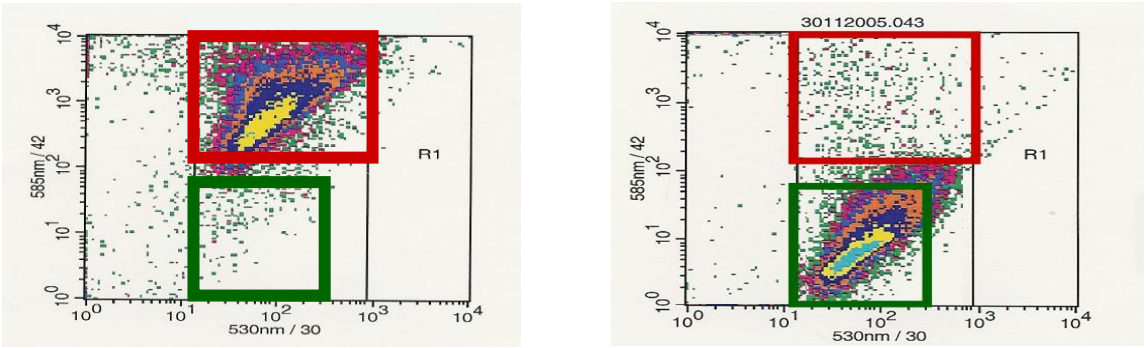

c

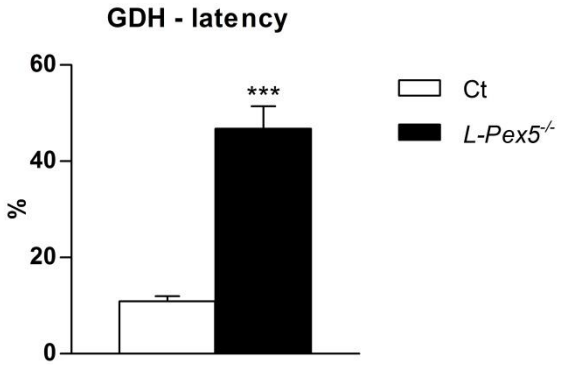

d

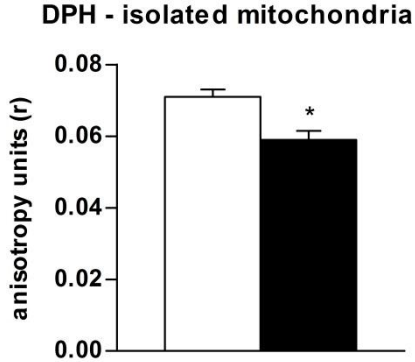

e

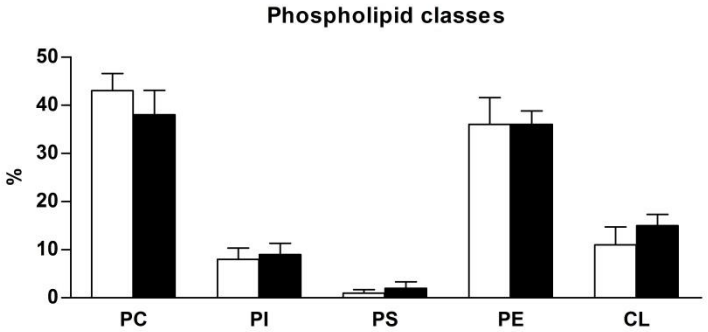

Figure 5

a

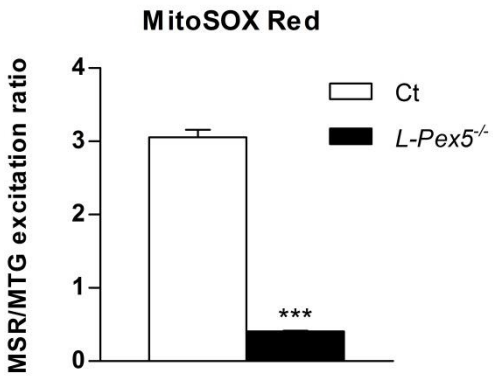
MitoSOX Red
MSR/MTG excitation ratio
4
3
2
1
0
***
Ct
L-Pex5-/-

b

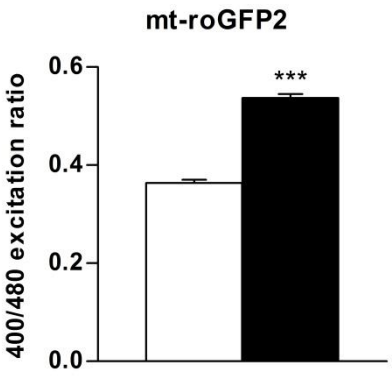
mt-roGFP2
400/480 excitation ratio
0.6
0.4
0.2
0.0
***

Figure 6

a

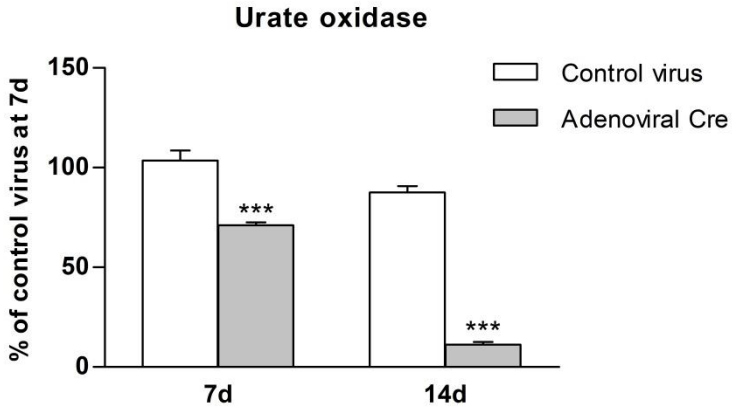

b

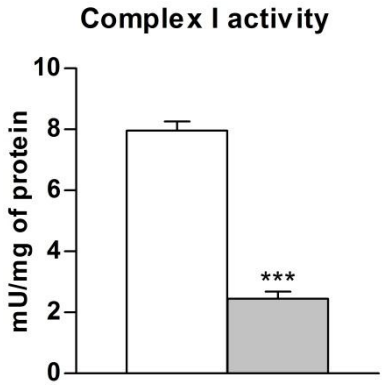

c

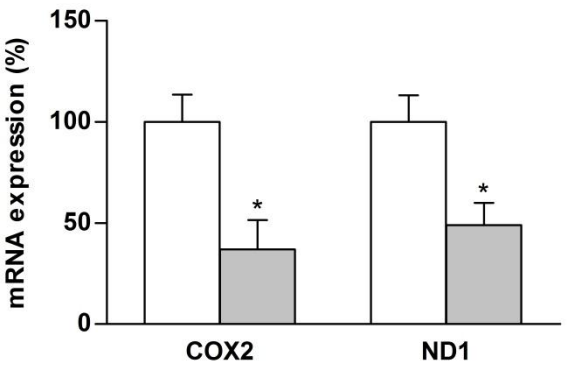

d

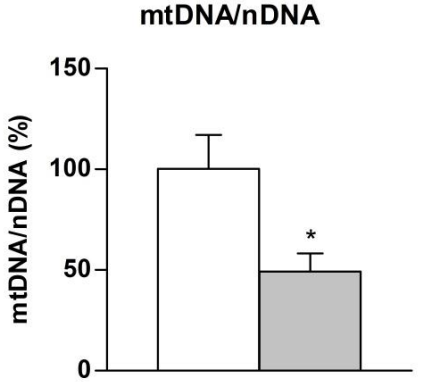

Figure 7

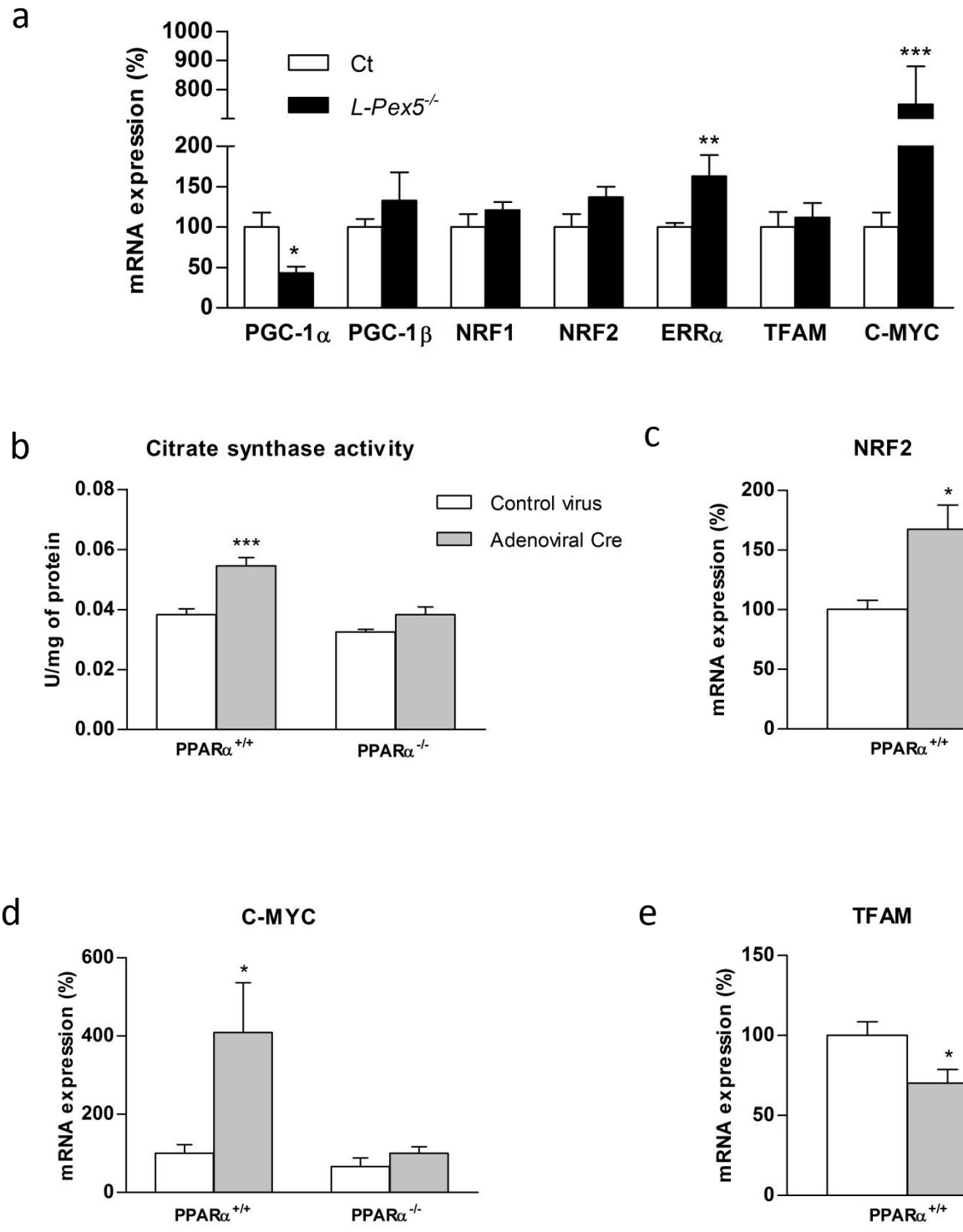
a
mRNA expression (%)
1000
900
800
200
150
100
50
0
Ct
L-Pex5-/-
*
**
***
PGC-1α
PGC-1β
NRF1
NRF2
ERRα
TFAM
C-MYC
b
Citrate synthase activity
U/mg of protein
0.08
0.06
0.04
0.02
0.00
Control virus
Adenoviral Cre
***
PPARα+/+
PPARα-/-
c
NRF2
mRNA expression (%)
200
150
100
50
0
*
PPARα+/+
d
C-MYC
mRNA expression (%)
600
400
200
0
*
PPARα+/+
PPARα-/-
e
TFAM
mRNA expression (%)
150
100
50
0
*
PPARα+/+